

Observation of two-orbital spin-exchange interactions with ultracold $SU(N)$ -symmetric fermions

F. Scazza,^{1,2} C. Hofrichter,^{1,2} M. Höfer,^{1,2} P. C. De Groot,^{1,2} I. Bloch,^{1,2} and S. Fölling^{1,2,*}

¹*Ludwig-Maximilians-Universität, Schellingstraße 4, 80799 München, Germany*

²*Max-Planck-Institut für Quantenoptik, Hans-Kopfermann-Straße 1, 85748 Garching, Germany*

(Dated: September 13, 2022)

We report on the direct observation of spin-exchanging interactions in a two-orbital $SU(N)$ -symmetric quantum gas of ytterbium in an optical lattice. The two orbital states are represented by two different (meta-)stable electronic configurations of fermionic ^{173}Yb . A strong spin-exchange between particles in the two separate orbitals is mediated by the contact interaction between atoms, which we characterize by clock shift spectroscopy in a 3D optical lattice. We find the system to be $SU(N)$ -symmetric within our measurement precision and characterize all relevant scattering channels for atom pairs in combinations of the ground and the excited state. Elastic scattering between the orbitals is dominated by the antisymmetric channel, which leads to the strong spin-exchange coupling. The exchange process is directly observed, by characterizing the dynamic equilibration of spin imbalances between two large ensembles in the two orbital states, as well as indirectly in atom pairs via interaction shift spectroscopy in a 3D lattice. The realization of a stable $SU(N)$ -symmetric two-orbital Hubbard Hamiltonian opens the route towards experimental quantum simulation of condensed-matter models based on orbital interactions, such as the Kondo lattice model.

PACS numbers: 34.50.Cx, 42.62.Fi, 75.10.Dg, 67.85.Lm

Ultracold gases of alkaline-earth-like atoms have recently been the focus of increasing theoretical [1] and experimental [2–5] efforts, owing to the versatile internal structure which makes them attractive candidates for the study of quantum many-body physics. One of the remarkable properties of alkaline-earth-like atoms is the existence of a long-lived metastable excited electronic state, due to the separate singlet and triplet electronic spin manifolds. The correspondingly low linewidths of the associated optical “clock” transitions has enabled the realization of the most precise atomic clocks [6, 7]. More recently, the existence of two stable electronic states has also inspired many proposals for the implementation of previously inaccessible fundamental many-body systems [1, 8] and quantum information processing schemes [9, 10]. These proposals are motivated by the fact that the two states, due to their different electronic configurations, have very different properties both in how the atom interacts with light and how it interacts with other atoms. This is in direct analogy to electrons in a crystal lattice which occupy two different orbitals, a vital part of fundamental condensed-matter models such as the Kondo lattice [11, 12] and the Kugel-Khomskii model [1]. Such models are used to describe a large class of materials, and rely on the coexistence of electrons in two orbitals and the existence of a spin-exchange coupling term between these. Using the electronic state to simulate the orbital degree of freedom has been proposed as a solution to the challenge of simulating such Hamiltonians.

A second striking property of alkaline-earth-like atoms is the large decoupling between electronic and nuclear degrees of freedom which is expected for states with total electronic angular momentum $J = 0$ [1, 13]. This re-

sults in an $SU(N)$ -symmetric situation, where collisional properties are independent of the nuclear spin orientation. Systems possessing such high-dimensional symmetries are predicted to exhibit a variety of still unexplored many-body phases [14–16]. In our case, using ^{173}Yb and choosing the metastable state $|e\rangle = ^3P_0$ as the second orbital in addition to the ground state $|g\rangle = ^1S_0$, is expected to realize a $SU(N)$ -symmetric two-orbital model. The existence of spin-exchanging coupling terms, which lie at the heart of orbital quantum magnetism, as well as the stability of the ensuing ensemble depend on specific properties of the interactions between $|g\rangle$ and $|e\rangle$ atoms, and have previously been unknown.

Interactions between ultracold Yb atoms in the electronic ground state are well characterized for most isotopes [17], as well as the relevant interaction processes which occur in atomic clock experiments making use of ^{171}Yb ($I = 1/2$) [18, 19]. More recently, the interaction strength between the ground state and the 3P_2 state of the bosonic ^{174}Yb ($I = 0$) isotope has been determined in an optical lattice [20, 21]. In the present work, we characterize the specific properties of the 1S_0 - 3P_0 interaction channels of the ^{173}Yb ($I = 5/2$) isotope and directly reveal their $SU(N)$ -symmetric nature. Most importantly, we experimentally demonstrate strong spin-exchanging interactions between atoms in the two different electronic states. The interaction channels are characterized by measuring interaction clock shifts, for different m_F state combinations and magnetic field strengths. The magnetic field causes a state mixing, leading to a novel tunability of one of the Hubbard model interaction parameters. Spin-exchanging collisions between the two electronic orbitals are observed directly in our system via the spin balance

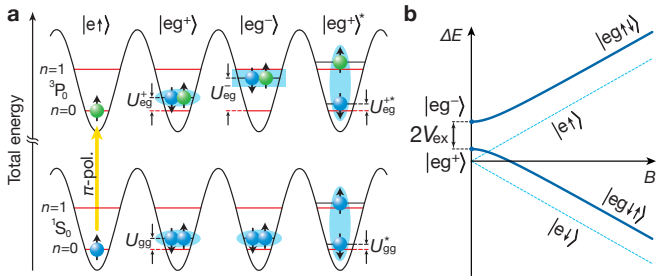


FIG. 1. **Two-orbital interacting states of fermions in a lattice.** (a) One- and two-particle states for interacting atoms on a lattice site with both orbital ($|g\rangle$: blue and $|e\rangle$: green) and nuclear spin ($|\uparrow\rangle, |\downarrow\rangle$) degrees of freedom. The corresponding energy levels are also illustrated. A blue ellipse (rectangle) indicates a nuclear spin singlet (triplet). (b) Sketch of the magnetic field dependence of the energy for an interacting atom pair on a lattice site (blue solid line). Energies of one-particle excited states are also drawn for comparison (dashed line). The zero here corresponds to the resonance of the clock transition for singly-occupied sites at zero magnetic field. For large Zeeman shifts ($|\Delta_B| \gg |V_{\text{ex}}|$) the two-particle eigenstates are the $|eg\uparrow\downarrow\rangle$ and $|eg\downarrow\uparrow\rangle$ states, as defined in the text.

evolution in large ensembles. Such spin-exchange interactions were observed for localized pairs of bosons in different motional states of a single lattice site [22]. Excited motional states however are not stable in the presence of strong tunnelling, a necessary component for realizing many-body systems such as the Kondo lattice model [1]. In contrast, the long lifetime of the metastable state in Yb is not compromised by a high mobility of one orbital, as long as the strongly inelastic collisions between two $|e\rangle$ -state atoms can be avoided.

The interactions between ground state atoms in an $SU(N)$ -symmetric degenerate ^{173}Yb gas can be fully characterized by a single s -wave scattering length $a_{gg} = 199.4a_0$ [17]: the scattering length is independent of the nuclear spin orientation, preventing therefore spin-changing collisions [23].

Moreover, p -wave collisions can typically be neglected, as they are strongly suppressed in the degenerate temperature regime. Introducing an additional internal degree of freedom, represented here by the electronic state, extends the system to a two-orbital description, where more collision channels become available. With the two electronic orbitals $|g\rangle$ and $|e\rangle$, four s -wave scattering lengths are sufficient to describe collision processes for all nuclear spin combinations due to the $SU(N)$ symmetry. The scattering lengths a_{gg} and a_{ee} apply to atom pairs in the states $|gg\rangle$ and $|ee\rangle$, where both atoms are in the same electronic states $|g\rangle$ and $|e\rangle$, respectively. In addition, interactions between atoms in different electronic states, which are responsible for spin exchange between orbitals, are described by two parameters a_{eg}^{\pm} for the symmetric and anti-symmetric combinations

$(|eg\rangle \pm |ge\rangle)/\sqrt{2}$. We consider the specific case of one g and one e atom in the lowest vibrational state of the same lattice site, with two different nuclear spin states $|\uparrow\rangle$ and $|\downarrow\rangle$, usually chosen to have opposite m_F values for simplicity. As the fermionic statistics enforces the total state to be anti-symmetric, two states are possible, which we denote as $|eg^+\rangle = (|eg\rangle + |ge\rangle)/\sqrt{2} \otimes |s\rangle$ and $|eg^-\rangle = (|eg\rangle - |ge\rangle)/\sqrt{2} \otimes |t\rangle$, where $|s\rangle$ and $|t\rangle$ are the nuclear spin singlet and triplet states. All the relevant states are illustrated in Fig. 1(a). Given the scattering lengths introduced above, the on-site Hubbard interaction strength for the different states can be written as:

$$U_X = \frac{4\pi\hbar^2}{m} a_X \int d^3r w_a^2(\mathbf{r}) w_b^2(\mathbf{r}), \quad (1)$$

where $X = gg, ee, eg^+, eg^-$. Here, m is the atomic mass and $w_{a,b}(\mathbf{r})$ are the Wannier functions of the two atoms. The above expression is valid in the regime of sufficiently weak interactions ($a_X \ll a_{\text{ho}}$, with a_{ho} being the on-site harmonic oscillator length), where the two-particle wavefunction can be expressed as a product of single-particle Wannier functions.

In addition to the interaction energy, we introduce a Zeeman energy contribution from an external magnetic field \mathbf{B} . It arises due to the differential Zeeman shift between the $|g\rangle$ and the $|e\rangle$ states with a given m_F [24] and causes the linear magnetic shift of single-atom $|g, m_F\rangle \rightarrow |e, m_F\rangle$ clock transitions. The magnetic field introduces a coupling between $|eg^+\rangle$ and $|eg^-\rangle$, as it breaks the spin up-down symmetry. The Hamiltonian for the two-atom system with a single electronic excitation can then be written in the $\{|eg^+\rangle, |eg^-\rangle\}$ basis, and has the form of a coupled two-level system

$$H_{eg} = \begin{pmatrix} U_{eg}^+ & \Delta_B \\ \Delta_B & U_{eg}^- \end{pmatrix}, \quad (2)$$

where $\Delta_B = \delta g m_F \mu_B B$ is the differential Zeeman shift. Here, δg is the differential nuclear Landé g -factor [24], m_F is the nuclear spin projection along the field and μ_B is the Bohr magneton. Diagonalization results in two eigenenergy branches, represented in Fig. 1(b):

$$E_{1,2} = V \pm \sqrt{V_{\text{ex}}^2 + \Delta_B^2}, \quad (3)$$

where $V = (U_{eg}^+ + U_{eg}^-)/2$ and $V_{\text{ex}} = (U_{eg}^+ - U_{eg}^-)/2$. The zero-field eigenstates are then $|eg^+\rangle$ and $|eg^-\rangle$, whereas for high fields their superpositions form the eigenbasis: $|eg\uparrow\downarrow\rangle = (|e\uparrow\rangle|g\downarrow\rangle - |g\downarrow\rangle|e\uparrow\rangle)/\sqrt{2}$, $|eg\downarrow\uparrow\rangle = (|e\downarrow\rangle|g\uparrow\rangle - |g\uparrow\rangle|e\downarrow\rangle)/\sqrt{2}$.

Our experimental procedure for the preparation of a degenerate Fermi gas is described in more detail in the Supplementary Information. After Zeeman slowing and cooling in a MOT, approximately 10^7 atoms of ^{173}Yb ($I = 5/2$) are loaded into a crossed optical dipole trap,

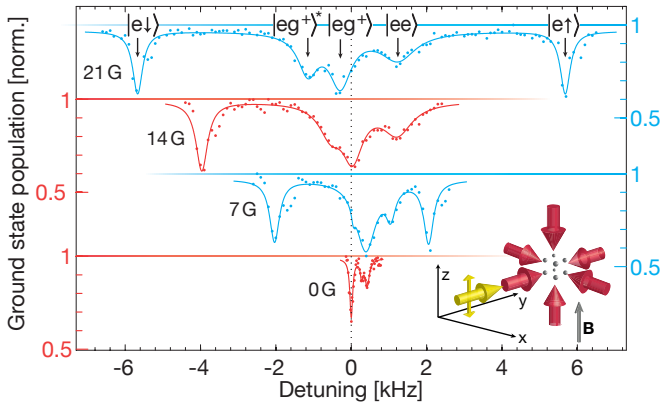


FIG. 2. **Clock transition spectroscopy of a two-component Fermi gas in a 3D lattice.** The absorption signals for the $m_F = \pm 5/2$ spin mixture are shown, displaying resonances corresponding to different final states. Solid lines are multiple-Lorentzian fits to determine the resonance positions. Singly-occupied lattice site resonances shift proportionally to the magnetic field due to the differential Zeeman shift between $|g\rangle$ and $|e\rangle$ states, whereas doubly-occupied site resonance shifts are dependent upon the final state of the excitation. An excitation light intensity of 7.5 mW/cm^2 was used in these experimental runs, except for the 0 G data where a reduced light intensity of 2.3 mW/cm^2 was used to improve the resolution. The experimental configuration is schematically represented in the lower-right corner.

where the desired spin mixture is prepared by optical pumping. Evaporative cooling is carried out until the gas reaches Fermi degeneracy, with typically $N \simeq 1 \times 10^5$ atoms at $T/T_F = 0.25(5)$. The cloud is then loaded into a deep 3D optical lattice operating at the state-independent (“magic”) wavelength of 759.354 nm [25]. Absorption imaging is performed using linearly polarized light, which minimizes the effect of the nuclear spin on the detection. Spin-resolved atom number detection is achieved by means of an optical Stern-Gerlach scheme, based on σ^+ -polarized blue-detuned light [23, 26] (see Supplementary Information). In order to probe the ultranarrow $^1S_0 \rightarrow ^3P_0$ transition at 578 nm , a laser is stabilized to a high-finesse ULE cavity reference, achieving an absolute stability of $\simeq 40 \text{ Hz}$. The probe beam is overlapped with one of the lattice axes and π -polarized along a uniform external \mathbf{B} field, so that the excitation does not change the nuclear spin state.

By loading a two-component gas into a 3D lattice, we obtain an average filling between $\bar{n} = 1$ and $\bar{n} = 2$ per lattice site and a temperature above the spin-1/2 Mott insulating transition. The interaction shift of the $^1S_0 \rightarrow ^3P_0$ transition then is a direct measurement of the difference between U_{gg} and U_{eg}^+ , as illustrated in Fig. 1(a). Without magnetic field or other symmetry-breaking effects, the initial state $|gg\rangle \otimes |s\rangle$ is only coupled to the $|eg^+\rangle$ state. An increasing magnetic field coupling changes the

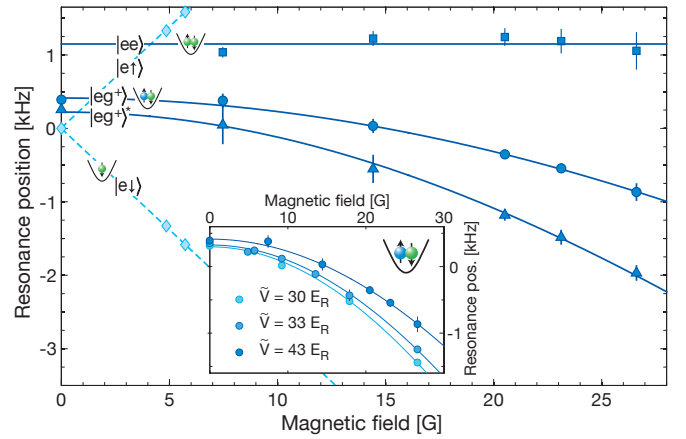


FIG. 3. **Magnetic field dependence of clock transition frequencies in the presence of two-orbital on-site interactions.** Resonance positions in an $m_F = \pm 5/2$ spin mixture are shown for $\tilde{V} = 43 E_R$, where $\tilde{V} = (V_x V_y V_z)^{1/3}$ is the mean lattice depth in units of recoil energy of the lattice. Squares mark transitions to $|ee\rangle$, circles to $|eg^+\rangle$, triangles to $|eg^+\rangle^*$ and diamonds to $|e\uparrow\rangle$ and $|e\downarrow\rangle$ states. Resonance shifts of $|eg^+\rangle$ and $|eg^+\rangle^*$ states are fitted according to the model in Eq. (3) (solid blue lines). The doubly-excited $|ee\rangle$ state resonance position does not shift with magnetic field, as the two differential Zeeman shifts cancel each other. Error bars are derived from Lorentz fit position uncertainties. Eq. (3) fit results for this lattice configuration are: $V_{\text{ex}} = h \cdot (-22.2 \pm 1.0) \text{ kHz}$ and $V = U_{gg} + h \cdot (22.6 \pm 1.9) \text{ kHz}$. Inset: the $|eg^+\rangle$ resonance shifts are plotted at varying magnetic field for three different lattice depths.

energy of the lower eigenstate of Eq. (2), and probing this dependence allows for determination of V_{ex} through Eq. (3). Scans of the probe laser detuning displaying various absorption lines in a $m_F = \pm 5/2$ spin mixture are shown in Fig. 2. The singly-occupied lattice sites are associated to the outermost resonances, which shift linearly with magnetic field strength. The frequency offset is calibrated using the center of these two resonances, which correspond to the single-atom transition frequency in the absence of a magnetic field. Three other absorption lines are clearly visible, associated to the excitation of doubly-occupied lattice sites. In Fig. 3 the positions of the different resonances are plotted as a function of the magnetic field for a $m_F = \pm 5/2$ spin mixture. We identify the strongest transition without linear Zeeman shift as the lower eigenstate of Eq. (3) and fit the resonance positions with V and V_{ex} as free parameters (see Supplementary Information). In this way we obtain the values of $U_{eg}^+ - U_{gg}$ and $U_{eg}^- - U_{gg}$ for each different lattice depth and spin mixture. From Eq. (1) and taking identical lowest-band Wannier functions for the two atoms, we calculate for each fit result of $U_{eg}^+ - U_{gg}$ the corresponding scattering length and obtain as mean value: $\Delta a_{eg}^+ = a_{eg}^+ - a_{gg} = (20.1 \pm 2.0) a_0$. However, fit estimates of U_{eg}^- exceed the energy gap to the first excited

band of the lattice, causing Eq. (1) to be inaccurate for computing the scattering length. A more suitable model including more bands is therefore required, which will be discussed below. Consistent values of Δa_{eg}^+ are obtained from spectroscopic measurements of several distinct spin mixtures, thereby demonstrating the $SU(N)$ symmetry of this scattering channel down to our experimental uncertainty of 0.9% of $a_{eg}^+ = 219.5a_0$. The reported value of Δa_{eg}^+ comprises all our measurements, including the case of all six nuclear spin states present. The magnetic field dependent shift of the transition is measured for all spin mixtures as well, yielding estimates of V_{ex} in good agreement with each other and therefore validating also the $SU(N)$ symmetry of the anti-symmetric scattering channel (see Supplementary Information). The two-particle spin-singlet nature of the $|eg^+\rangle$ resonance is also confirmed by the fact that we find that the Rabi frequency is larger than on the bare atom resonance by the expected factor of $\sqrt{2}$.

An additional absorption line is detected close to the $|eg^+\rangle$ line, which we associate with the final state $|eg^+\rangle^*$, schematically represented in Fig. 1(a). This transition is analogous to the $|gg\rangle \rightarrow |eg^+\rangle$ transition with both states having one excitation to the first excited vibrational state. The energy of this final state also depends on the magnetic field as described by Eq. (3). Fitting the data and using Eq. (1), in this case with different Wannier functions for the two atoms, yields $\Delta a_{eg}^+ = (22.7 \pm 7.3)a_0$, consistent with the value obtained from the $|eg^+\rangle$ resonance. We find this line to have a significant weight when high atom numbers are used, suggesting that the loading to the 3D lattice then is not fully adiabatic and the second band starts to become populated. Finally, we identify the resonance which exhibits no magnetic field shift with the transition to the $|ee\rangle$ state, corresponding to a detuned two-photon transition with $|eg^+\rangle$ as the intermediate state. Its coupling strength is therefore dependent on the separation to the $|eg^+\rangle$ line and its position is also insensitive to the spin mixture. Applying Eq. (1) to data for each spin combination separately, we obtain a mean value $\Delta a_{ee} = a_{ee} - a_{gg} = (106.8 \pm 10.4)a_0$. A direct excitation resonance to the $|eg^-\rangle$ state was not identified. Its strength is expected to be suppressed by the Lamb-Dicke effect and for, our low magnetic fields, due to the fact that a transition from nuclear singlet to triplet state is required. In addition, its location is expected close to the band excitation energy, in very close proximity to the blue Raman sidebands of the $|eg^+\rangle$ and single atom transitions.

The values of V_{ex} obtained by making use of the simple model in Eq. (3) are as large as $V_{ex} \simeq h \cdot 22$ kHz, corresponding to $U_{eg}^- \gtrsim h \cdot 44$ kHz, in comparison to a typical lattice band gap of only $\simeq h \cdot 25$ kHz, depending on the lattice configuration. In such a regime the strong interaction couples the excited bands of the lattice [27, 28], and the full band structure as well as proper regulariza-

tion of the interaction potential therefore has to be taken into account. As a consequence, the single-band model in Eqs. (1)-(3) breaks down: the anti-symmetric onsite pair wavefunction is modified by the strong U_{eg}^- interaction. For increasing interaction strengths, the wavefunction overlap between the two atoms is reduced compared to the lowest band Wannier function, up to the point where the atom pair “fermionizes”: for an infinite scattering length the interaction integral vanishes and the total energy saturates to the first excited band energy independent of the exact scattering length [29, 30]. Using Eq. (1) in this regime ($a_{eg}^- > a_{ho}$) for a given value of U therefore strongly underestimates the scattering length [27]. Applying Eq. (1) yields $\Delta a_{eg}^- = a_{eg}^- - a_{gg} = (1.97 \pm 0.19) \times 10^3 a_0$, which should be then taken only as a lower bound estimate. A numerical diagonalization including four bands, using an unregularized delta-potential was carried out, for which we find a larger value $\Delta a_{eg}^- \simeq 4 \times 10^3 a_0$ to best reproduce the data (see Supplementary Information). We also compared the data to the case of an infinite scattering length a_{eg}^- , thereby assuming full “fermionization” of the on-site wave function. Using the band gap energy for U_{eg}^- , which corresponds to the analytic result of the regularized treatment, the calculated magnetic field dependence of the lower eigenenergy branch is still close to the measured data, also implying a very large $a_{eg}^- > a_{ho}$. In this regime, the scattering length dependence of the signal is low and very precise modeling of the system including proper regularization, the complete internal structure and the full anisotropic lattice appears necessary to constrain the scattering length further when using on-site interaction data.

It can be easily seen that the interaction energy difference between the $|eg^+\rangle$ and $|eg^-\rangle$ state causes spin exchange can be easily seen when considering the product state $|eg^{\uparrow\downarrow}\rangle$, which is a superposition of $|eg^+\rangle$ and $|eg^-\rangle$. The energy difference between these two states then causes oscillations at zero magnetic field with a frequency equal to $|V_{ex}|/h$, between the $|eg^{\uparrow\downarrow}\rangle$ and $|eg^{\downarrow\uparrow}\rangle$ states, in analogy to the harmonic oscillator states in [22]. In order to generate the necessary superposition of $|eg^+\rangle$ and $|eg^-\rangle$ eigenstates at zero field, very large optical couplings Ω on the order of V_{ex}/h would be required. Alternatively, excitation in a large magnetic field and subsequently non-adiabatically switching to zero field would require a switching timescale $\ll h/|V_{ex}|$. In our setup both options can not be achieved due to the very large measured V_{ex} .

In order to still directly observe the dynamics driven by the exchange coupling directly, we use a different configuration with lower pair interaction strengths. Ensembles of atoms are loaded into 2D traps formed by a single, vertical standing wave and the excitation beam is also directed along the vertical axis (see Fig. 4(a)). We prepare a mixture of $|g^{\uparrow}\rangle$ and $|e^{\downarrow}\rangle$ atoms by magnetically

splitting the transitions to the $|e\uparrow\rangle$ and $|e\downarrow\rangle$ states in a degenerate two-component ($m_F = \pm 5/2$) Fermi gas, and addressing only the $|\downarrow\rangle$ state with a 0.2 ms π -pulse. The transition center is blue-shifted by typically $\simeq 0.5$ kHz with respect to the same transition in a spin-polarized gas due to the interaction shift. Subsequently, the magnetic field is rapidly reduced in 200 μ s to a low value and the atoms are held in the vertical lattice for a variable time. The spin distribution is detected by switching off the lattice and imaging after a 14 ms time of flight in combination with an optical Stern-Gerlach scheme.

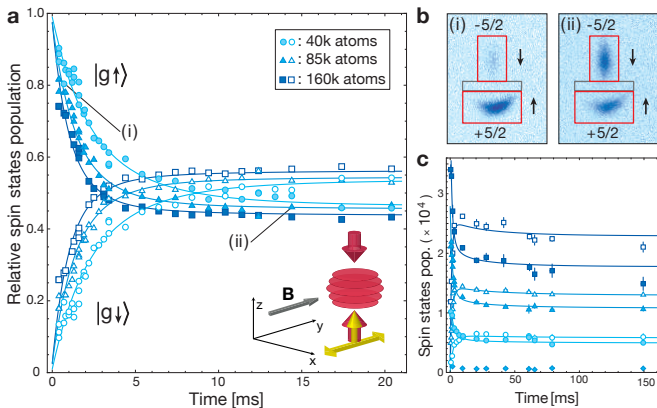


FIG. 4. **Spin-exchange dynamics between $|g\rangle$ and $|e\rangle$ atoms in 2D ensembles.** (a) The relative population of the two ground states $|g\uparrow\rangle$ ($m_F = +5/2$) and $|g\downarrow\rangle$ ($m_F = -5/2$) in a 1 G bias field is shown for variable hold times, after preparation in an approximately equal mixture of $|g\uparrow\rangle$ and $|e\downarrow\rangle$. The fitted curves are obtained with a two-body rate equation model that includes inelastic losses. The modified experimental configuration is schematically represented in the lower-right corner. (b) Examples of spin-resolved absorption images: 0.4 ms hold time (i) and 14 ms hold time (ii). Atom counting regions for the different spin states are shown: the solid red rectangles correspond to atoms occupying the $m_F = \pm 5/2$ states, the grey rectangle corresponds to atoms occupying other intermediate spin states. (c) Long-time evolution of the spin distribution: a weak loss of ground state atoms due to inelastic collisions is visible. Intermediate spin state populations are shown as filled diamonds for the $N = 0.85 \times 10^5$ atoms case. No re-population of other spin states is detected. Error bars denote the statistical errors obtained by binning several data points.

As expected for a situation with a large exchange interaction, we observe a fast redistribution of the two spin components as soon as the bias field is reduced to a small value of 1 G. The equilibration takes place without populating any other spin state, indicating genuine spin-exchange between the two electronic states in the absence of spin-changing collisions and further confirming therefore the $SU(N)$ symmetric character of this process. We fit the spin state population evolution with a two-body rate equation model, which assumes resonant spin-exchange and includes fast inelastic $e-e$ collisional losses for atoms in different spin states and a low $e-g$

loss rate coefficient (see Supplementary Information). We find the spin-exchange dynamics to be very fast and the re-balancing of the spin distribution starts already while the magnetic field is being ramped to the hold value. For long holding times, the spin distribution reaches a stationary ratio according to the spin distribution prior to excitation.

Fits to the data obtained for a set of three different atom numbers are shown in Fig. 4. Based on a finite-temperature density model of the 2D trapped gas in each of the vertical lattice sites, the fits yield a spin-exchange rate value $\gamma_{ex} = (1.2 \pm 0.2) \times 10^{-11} \text{ cm}^3/\text{s}$.

Inelastic $e-e$ state losses are independently measured by applying a π -pulse to a gas loaded into the vertical optical lattice at zero magnetic field, exciting therefore an equal portion of both spin states. After the residual ground state atoms are removed by a blast pulse resonant with the strong 1P_1 transition, the excited atomic population is monitored at varying hold time, by mapping it back to the ground state with a second π -pulse. An inelastic loss rate $\beta_{ee} = (2.2 \pm 0.5) \times 10^{-11} \text{ cm}^3/\text{s}$ is estimated, based on the same density model used for the spin-exchange rate estimation and in reasonable agreement with previous measurements [18]. Inelastic $g-e$ state losses are also characterized by a similar independent measurement (see Supplementary Informations). Fits to this data and to the data in Fig. 4(c) yield a loss rate coefficient $\beta_{eg} = (6.0 \pm 1.4) \times 10^{-13} \text{ cm}^3/\text{s}$, which includes both symmetric and antisymmetric channels. The uncertainties of the three reported rate coefficients are due to uncertainties in the determination of the in-plane densities. The spin distribution evolutions obtained by rate equation fits are displayed as solid lines in Fig. 4(a)-(c).

In conclusion, we realize a two-orbital $SU(N)$ -symmetric system and characterize the relevant interaction properties of ^{173}Yb through high-resolution interaction spectroscopy in a 3D optical lattice. By direct observation of spin-exchange dynamics in 2D ensembles, a very strong magnetic coupling between the two electronic orbitals is demonstrated. The strong interaction found in our work is highly desirable for the implementation of orbital quantum magnetic phases, as tuning to lower values can always be achieved by reducing the overlap between the e and g lattice potentials [9]. The direct observation of orbital spin exchange, the elementary building block of orbital quantum magnetism, therefore is a fundamental step towards the realization of paradigmatic phases of matter and their $SU(N)$ -symmetric extensions.

We gratefully acknowledge contributions by C. Schweizer, E. Davis and P. Ketterer during the construction of the experiment, and helpful discussions with A.M. Rey, M. Wall and A. Daley. This work was supported by the EU through the UQAM program.

During the preparation of this manuscript, we became aware of related work by Zhang *et al.* in ^{87}Sr [31].

* simon.foelling@lmu.de

- [1] A. V. Gorshkov, M. Hermele, V. Gurarie, C. Xu, P. S. Julienne, J. Ye, P. Zoller, E. Demler, M. D. Lukin, and A. M. Rey. Two-orbital SU(N) magnetism with ultracold alkaline-earth atoms. *Nature Physics* **6**, 289–295 (2010).
- [2] S. Sugawa, K. Inaba, S. Taie, R. Yamazaki, M. Yamashita, and Y. Takahashi. Interaction and filling-induced quantum phases of dual Mott insulators of bosons and fermions. *Nature Physics* **7**, 642–648 (2011).
- [3] S. Taie, R. Yamazaki, S. Sugawa, and Y. Takahashi. An SU(6) Mott insulator of an atomic Fermi gas realized by large-spin Pomeranchuk cooling. *Nature Physics* **8**, 825–830 (2012).
- [4] M. Martin, M. Bishof, M. Swallows, X. Zhang, C. Benko, J. von Stecher, A. Gorshkov, A. Rey, and J. Ye. A quantum many-body spin system in an optical lattice clock. *Science* **341**, 632–636 (2013).
- [5] G. Pagano, M. Mancini, G. Cappellini, P. Lombardi, F. Schäfer, H. Hu, X.-J. Liu, J. Catani, C. Sias, M. Inguscio, et al. A one-dimensional liquid of fermions with tunable spin. *Nature Physics* **10**, 198–201 (2014).
- [6] N. Hinkley, J. A. Sherman, N. B. Phillips, M. Schioppa, N. D. Lemke, K. Beloy, M. Pizzocaro, C. W. Oates, and A. D. Ludlow. An Atomic Clock with 10^{-18} Instability. *Science* **341**, 1215–1218 (2013).
- [7] B. Bloom, T. Nicholson, J. Williams, S. Campbell, M. Bishof, X. Zhang, W. Zhang, S. Bromley, and J. Ye. An optical lattice clock with accuracy and stability at the 10^{-18} level. *Nature* (2014).
- [8] F. Gerbier and J. Dalibard. Gauge fields for ultracold atoms in optical superlattices. *New Journal of Physics* **12**, 033007 (2010).
- [9] A. J. Daley, M. M. Boyd, J. Ye, and P. Zoller. Quantum Computing with Alkaline-Earth-Metal Atoms. *Phys. Rev. Lett.* **101**, 170504 (2008).
- [10] A. V. Gorshkov, A. M. Rey, A. J. Daley, M. M. Boyd, J. Ye, P. Zoller, and M. D. Lukin. Alkaline-earth-metal atoms as few-qubit quantum registers. *Physical review letters* **102**, 110503 (2009).
- [11] M. Foss-Feig, M. Hermele, and A. M. Rey. Probing the Kondo lattice model with alkaline-earth-metal atoms. *Phys. Rev. A* **81**, 051603 (2010).
- [12] M. Foss-Feig, M. Hermele, V. Gurarie, and A. M. Rey. Heavy fermions in an optical lattice. *Phys. Rev. A* **82**, 053624 (2010).
- [13] M. M. Boyd, T. Zelevinsky, A. D. Ludlow, S. M. Foreman, S. Blatt, T. Ido, and J. Ye. Optical atomic coherence at the 1-second time scale. *Science* **314**, 1430–1433 (2006).
- [14] M. Hermele, V. Gurarie, and A. M. Rey. Mott Insulators of Ultracold Fermionic Alkaline Earth Atoms: Underconstrained Magnetism and Chiral Spin Liquid. *Physical Review Letters* **103**, 135301 (2009).
- [15] M. Cazalilla, A. Ho, and M. Ueda. Ultracold gases of ytterbium: Ferromagnetism and Mott states in an SU(6) Fermi system. *New Journal of Physics* **11**, 103033 (2009).
- [16] C. Honerkamp and W. Hofstetter. Ultracold Fermions and the SU(N) Hubbard Model. *Phys. Rev. Lett.* **92**, 170403 (2004).
- [17] M. Kitagawa, K. Enomoto, K. Kasa, Y. Takahashi, R. Ciuryło, P. Naidon, and P. S. Julienne. Two-color photoassociation spectroscopy of ytterbium atoms and the precise determinations of s-wave scattering lengths. *Physical Review A* **77**, 012719 (2008).
- [18] A. D. Ludlow, N. D. Lemke, J. A. Sherman, C. W. Oates, G. Quémener, J. von Stecher, and A. M. Rey. Cold-collision-shift cancellation and inelastic scattering in a Yb optical lattice clock. *Phys. Rev.* **A84**, 052724 (2011).
- [19] N. D. Lemke, J. von Stecher, J. A. Sherman, A. M. Rey, C. W. Oates, and A. D. Ludlow. p-Wave Cold Collisions in an Optical Lattice Clock. *Physical Review Letters* **107**, 103902 (2011).
- [20] A. Yamaguchi, S. Uetake, D. Hashimoto, J. M. Doyle, and Y. Takahashi. Inelastic Collisions in Optically Trapped Ultracold Metastable Ytterbium. *Physical Review Letters* **101**, 233002 (2008).
- [21] S. Kato, S. Sugawa, K. Shibata, R. Yamamoto, and Y. Takahashi. Control of Resonant Interaction between Electronic Ground and Excited States. *Phys. Rev. Lett.* **110**, 173201 (2013).
- [22] M. Anderlini, P. J. Lee, B. L. Brown, J. Sebby-Strabley, W. D. Phillips, and J. V. Porto. Controlled exchange interaction between pairs of neutral atoms in an optical lattice. *Nature* **448**, 452–456 (2007).
- [23] S. Stellmer, R. Grimm, and F. Schreck. Detection and manipulation of nuclear spin states in fermionic strontium. *Phys. Rev. A* **84**, 043611 (2011).
- [24] M. M. Boyd, T. Zelevinsky, A. D. Ludlow, S. Blatt, T. Zanon-Willette, S. M. Foreman, and J. Ye. Nuclear spin effects in optical lattice clocks. *Phys. Rev. A* **76**, 022510 (2007).
- [25] Z. W. Barber, J. E. Stalnaker, N. D. Lemke, N. Poli, C. W. Oates, T. M. Fortier, S. A. Diddams, L. Hollberg, C. W. Hoyt, A. V. Taichenachev, and V. I. Yudin. Optical Lattice Induced Light Shifts in an Yb Atomic Clock. *Phys. Rev. Lett.* **100**, 103002 (2008).
- [26] S. Taie, Y. Takasu, S. Sugawa, R. Yamazaki, T. Tsujimoto, R. Murakami, and Y. Takahashi. Realization of a SU(2)×SU(6) system of fermions in a cold atomic gas. *Phys. Rev. Lett.* **105**, 190401 (2010).
- [27] T. Busch, B. Englert, K. Rzȃzewski, and M. Wilkens. Two Cold Atoms in a Harmonic Trap. *Foundations of Physics* **28**, 549–559 (1998).
- [28] S. Will, T. Best, U. Schneider, L. Hackermüller, D.-S. Lühmann, and I. Bloch. Time-resolved observation of coherent multi-body interactions in quantum phase revivals. *Nature* **465**, 197–201 (2010).
- [29] B. Paredes, A. Widera, V. Murg, O. Mandel, S. Fölling, I. Cirac, G. V. Shlyapnikov, T. W. Hänsch, and I. Bloch. Tonks-Girardeau gas of ultracold atoms in an optical lattice. *Nature* **429**, 277–281 (2004).
- [30] G. Zürn, F. Serwane, T. Lompe, A. N. Wenz, M. G. Ries, J. E. Bohn, and S. Jochim. Fermionization of Two Distinguishable Fermions. *Phys. Rev. Lett.* **108**, 075303 (2012).
- [31] X. Zhang, M. Bishof, S. L. Bromley, C. V. Kraus, M. S. Safronova, P. Zoller, A. M. Rey, and J. Ye. Direct observation of SU(N) orbital magnetism. Preprint at <http://arxiv.org/abs/1403.2964> (2014).

Supplementary Information:

Observation of two-orbital spin-exchange interactions
with ultracold $SU(N)$ -symmetric fermions

F. Scazza^{1,2}, C. Hofrichter^{1,2}, M. Höfer^{1,2}, P. C. de Groot^{1,2}, I. Bloch^{1,2} & S. Fölling^{1,2}

¹ Fakultät für Physik, Ludwig-Maximilians-Universität,
Schellingstrasse 4, 80799 München, Germany

² Max-Planck-Institut für Quantenoptik,
Hans-Kopfermann-Strasse 1, 85748 Garching, Germany

EXPERIMENTAL SEQUENCE

Atoms of ^{173}Yb ($I = 5/2$) out of a thermal beam are first slowed on the strong $^1S_0 \rightarrow ^1P_1$ transition ($\Gamma/2\pi = 29$ MHz) at 399 nm. The decelerated atoms are collected and cooled in a MOT, working on the narrow intercombination $^1S_0 \rightarrow ^3P_1$ transition ($\Gamma/2\pi = 182$ kHz) at 556 nm. After a loading time of 8 s, the power and the detuning from resonance of the MOT beams are decreased in 50 ms, to let atoms cool down to a temperature $T \simeq 20$ μK . An optical dipole trap formed by two crossed beams at 1064 nm is then superimposed to the MOT and approximately 10^7 atoms are loaded into the trap in 200 ms. During the initial stage of the evaporation, the nuclear spin distribution is manipulated by means of optical pumping. A magnetic field of 20 G is applied in order to split the different hyperfine transitions of the $^1S_0 \rightarrow ^3P_1$ ($F = 5/2 \rightarrow F' = 7/2$) line. A σ^+ -polarized and a σ^- -polarized light beam at 556 nm are then used to independently address $m_F \rightarrow m_F \pm 1$ transitions and prepare the desired spin mixture by multiple light pulses. Clock transition spectroscopy runs are performed to reference the absolute frequency in completely spin-polarized samples with low atom number, in order to exclude any interaction-induced shifts. Evaporative cooling is carried out for 15 s, typically reaching a temperature $T/T_F = 0.25(5)$ at $N \simeq 10^5$ atoms, and the cloud is then loaded into an optical lattice operating at the magic wavelength 759.354 nm. Absorption imaging is performed using a linearly polarized light pulse resonant with the $^1S_0 \rightarrow ^1P_1$ transition. In order to separately detect the population of the different nuclear spin states, an optical Stern-Gerlach (OSG) scheme is used: a σ -polarized 556 nm light pulse with $\simeq 850$ MHz blue detuning from the $^1S_0 \rightarrow ^3P_1$ ($F = 5/2 \rightarrow F' = 7/2$) is shone on the atoms for 4 ms, with the maximum intensity gradient located at the atomic cloud center. Time-of-flight images with the application of the optical Stern-Gerlach scheme are shown in Fig. S1 for various spin mixture preparations. The ground state $SU(N)$ symmetry is verified by monitoring the collisional stability of a two-component degenerate spin mixture in the dipole trap: no spin relaxation induced by spin-changing collisions is detected after up to 15 s of holding time.

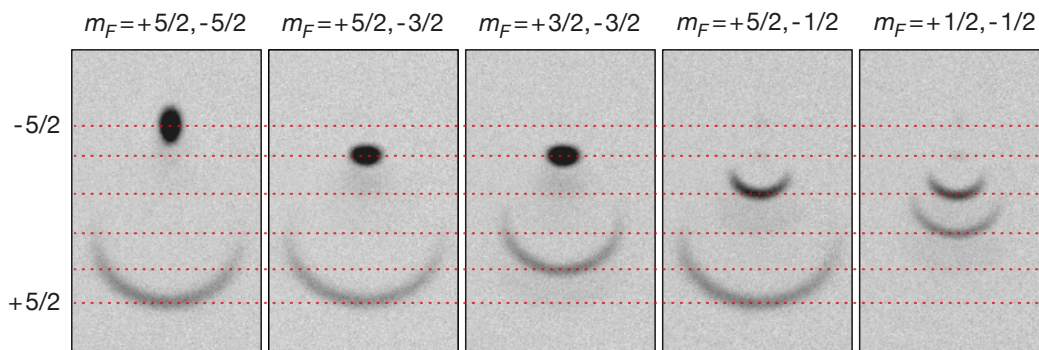


FIG. S1. **Time-of-flight absorption imaging of two-component Fermi gases with OSG.** Spin resolved images of different spin mixtures which were used in the reported measurements. A 4 ms OSG pulse is employed, with 30 mW light power and 80 μm waist at the atoms position.

The experimental sequence used for the observation of spin exchange in 2D ensembles is schematically illustrated in Fig. S2. Atoms are loaded into the vertical optical lattice in 200 ms and a clock transition π -pulse is used to prepare a balanced $|g\uparrow\rangle - |e\downarrow\rangle$ mixture. The spin dynamics is initiated by ramping the magnetic field to 1 G in 200 μs . After a

variable holding time, the magnetic field is ramped back up and the relative occupation of the spin states is detected by time-of-flight OSG imaging directly out of the lattice.

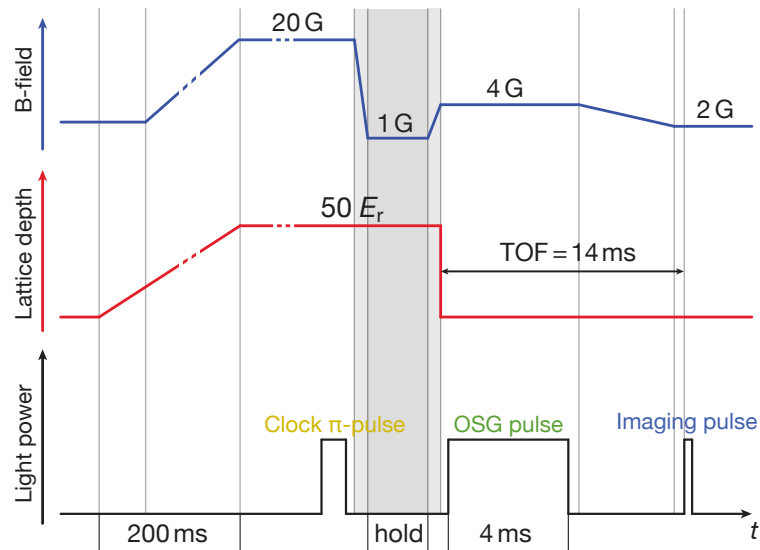


FIG. S2. Experimental sequence for the observation of spin-exchange dynamics in a 1D optical lattice.

DETERMINATION OF EXCHANGE ENERGY AND $SU(N)$ SYMMETRY

As described in the main text, the transition to the lower eigenstate of Eq. (2) exhibits a magnetic field dependence, which in a single-band model is given by Eq. (3). By fitting with Eq. (3) we obtain V and V_{ex} , and consequently $U_{eg}^+ - U_{gg}$ and $U_{eg}^- - U_{gg}$. A summary of results, corresponding only to the measurements of a $m_F = \pm 5/2$ mixture for three different lattice depths (shown in the inset of Fig. 3 in the main text), is given in Table S1.

$(V_x V_y V_z)^{1/3} [E_r]$	$U_{eg}^+ - U_{gg} [h \cdot \text{kHz}]$	$V_{\text{ex}} [h \cdot \text{kHz}]$	$U_{eg}^- - U_{gg} [h \cdot \text{kHz}]$
30	0.28 ± 0.14	-14.73 ± 2.40	29.75 ± 4.80
33	0.33 ± 0.05	-16.16 ± 0.83	32.65 ± 1.65
43	0.37 ± 0.05	-22.25 ± 0.95	44.87 ± 1.89

TABLE S1. Fit results for the $m_F = \pm 5/2$ mixture at different lattice depths.

Data for the transitions to the lower eigenstate and to the $|ee\rangle$ state in different spin mixtures are shown in Fig. S3-S4. The values of a_{eg}^+ , a_{ee} and the respective uncertainties given in the main text are estimated through the data points shown here. A very good agreement is found between parameter results associated to different spin mixtures, demonstrating the $SU(N)$ -symmetric nature of these interaction channels.

A generalization of Eq. (3) to arbitrary nuclear spin states m_F and m'_F is used in order to determine the resonance shifts in the curves of Fig. S3-S4:

$$h \cdot \Delta\nu(B) = \frac{1}{2} (m_F + m'_F) \delta g \mu_B B + (V - U_{gg}) - \sqrt{V_{\text{ex}}^2 + \left(\frac{1}{2} (m_F - m'_F) (\delta g \mu_B B) \right)^2} \quad (\text{S.1})$$

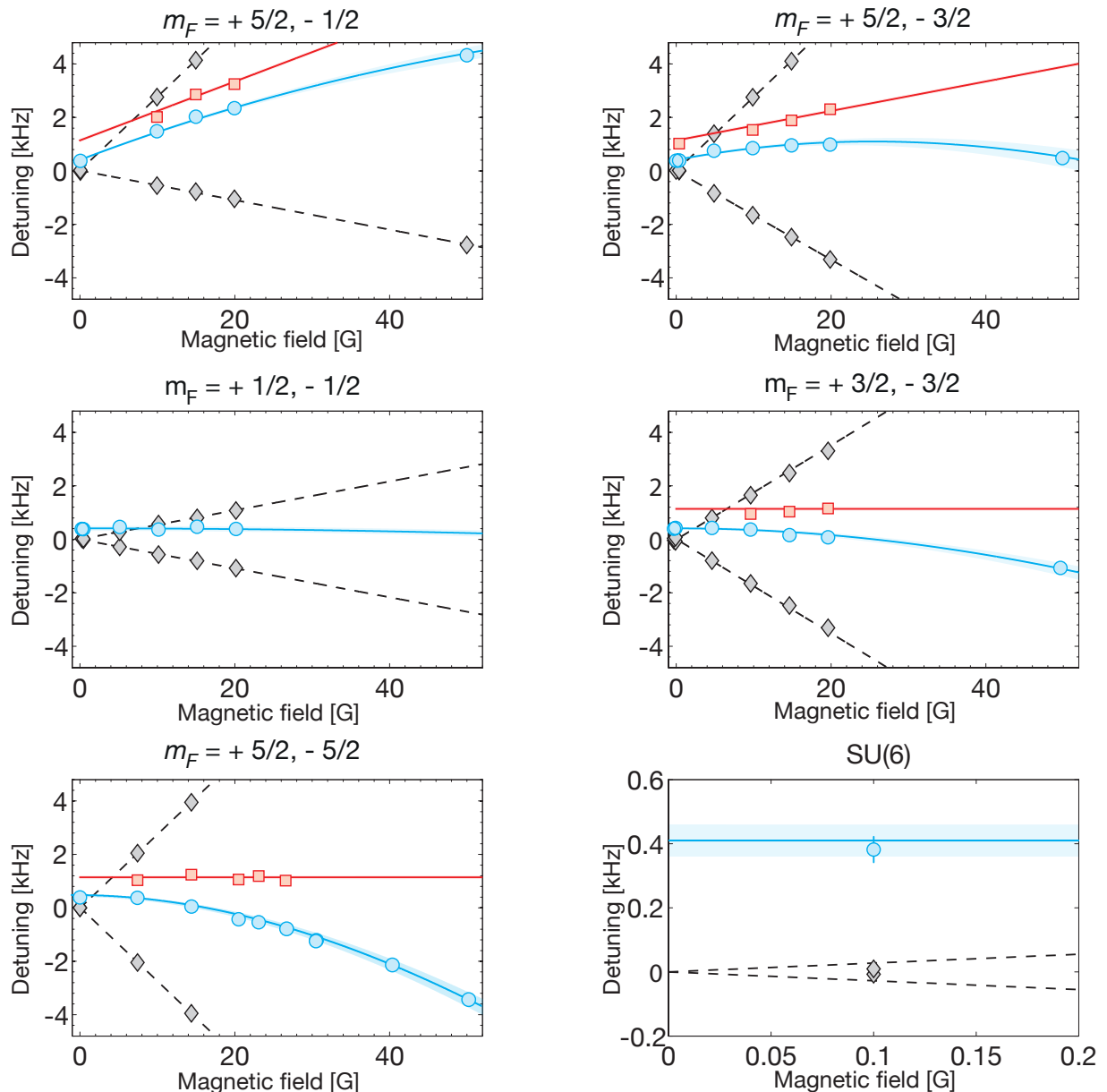


FIG. S3. **Resonance position shifts at varying magnetic field in different spin mixtures.** Grey diamonds mark singly-occupied site resonances, blue circles mark resonances to the lower eigenstate of Eq. (2), and red squares mark $|ee\rangle$ state resonances. The lattice depth is $\tilde{V} = 42.5E_r$. Solid blue lines are obtained through Eq. (S.1). Solid red lines correspond to the value of U_{ee} obtained through Eq. (1) using a_{ee} given in the main text. Shaded areas correspond to fit uncertainties. Data error bars correspond to Lorentz fit position uncertainties and are mostly hidden by data points.

For all blue curves in Fig. S3, the $V - U_{gg}$ and V_{ex} parameters obtained from the $m_F = \pm 5/2$ mixture data are being used. These are the ones with the smallest uncertainty amongst the fit results from all spin mixtures which are used in the experiment. All data sets are completely consistent with these fit results, validating the $SU(N)$ -symmetric character of U_{eg}^- as well. The solid red lines in Fig. S3 are determined using a single value of U_{ee} , obtained by inserting the estimated a_{ee} given in the main text into Eq. (1).

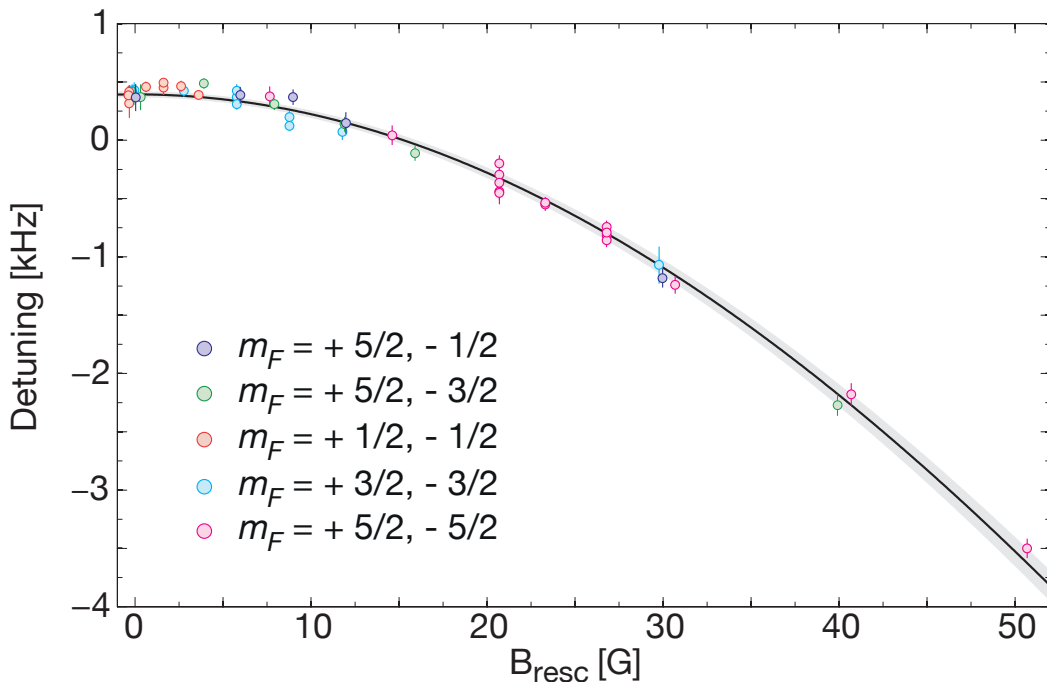


FIG. S4. **Shift of the transition to the lower eigenstate of Eq. (2) in different spin mixtures.** The data shown here corresponds to lattice depths in a range between $\tilde{V} = 41E_r$ and $\tilde{V} = 43E_r$. The magnetic field axis has been rescaled to $B_{\text{resc}} = \frac{1}{5}(m_F - m'_F)B$ and the linear Zeeman shift of spin mixtures with $m'_F \neq -m_F$ has been subtracted. The black solid curve is obtained through a fit of all data points with Eq. (S.1), and the shaded area around the curve corresponds to the fit uncertainty. Data error bars correspond to Lorentz fit position uncertainties.

MULTIBAND MODEL FOR STRONG INTERACTIONS

In order to account for the large antisymmetric interaction strength U_{eg}^- which we experimentally detect, it is necessary to take higher lattice bands into account to accurately estimate the interaction strength and the associated scattering length a_{eg}^- .

We performed a numerical diagonalization of the Hamiltonian including the lowest four energy bands of the lattice. The total Hamiltonian is given by:

$$\hat{H} = \hat{H}_{\text{at},2} \otimes \mathbb{1} + \mathbb{1} \otimes \hat{H}_{\text{lat},2} + \hat{U}, \quad (\text{S.2})$$

where the first Hilbert subspace refers to atom internal degrees of freedom (electronic and nuclear spin state) and the second Hilbert subspace refers to the motional degree of freedom (lattice vibrational states). The first term in the total Hamiltonian (S.2) accounts thus for the atom internal state, the second term for vibrational excitations and the third term for onsite contact interactions. The basis of completely symmetrized/anti-symmetrized two-particle states was used to numerically compute the Hamiltonian, where the interaction matrix elements were derived from computing the overlaps of onsite spatial wavefunctions of single-particle states. In order to remove bosonic states from the final solution an artificial large energy offset is added to all the symmetric states. The scattering length a_{eg}^+ was fixed to the measured value, whereas the scattering length a_{eg}^- was adjusted to make the lowest eigenenergy of (S.2) best reproduce the experimental data for the $m_F = \pm 5/2$ mixture.

In our four-band numerical diagonalization, a non-regularized Dirac delta contact potential was used, and this is expected to significantly underestimate the eigenenergies with respect to their true value [S1]. In order to obtain accurate values of the scattering lengths from on-site interaction shifts a more precise treatment is required [S1, S2, S3], which in this case would require the inclusion of the additional internal states.

IN-PLANE DENSITY MODEL IN A 1D OPTICAL LATTICE

In order to estimate the density of the 2D trapped gas in each of the vertical optical lattice sites, we use a model which assumes conservation of total entropy and thermal equilibrium during the loading from the dipole trap into the lattice. The profile of the Fermi gas in the dipole trap before the transfer into the lattice is modeled by a finite-temperature distribution obtained by local density approximation and valid in the limit of weak interaction. The trap frequencies are determined experimentally by transferring momentum to the atom cloud and measuring the sloshing frequency in the dipole trap. For the trap configuration as it is at the transfer into the optical lattice we measure the following frequencies: $\omega_x = 2\pi \cdot 8(1)$ Hz, $\omega_y = 2\pi \cdot 27(1)$ Hz and $\omega_z = 2\pi \times 212(5)$ Hz. After transfer into the lattice, the vertical degree of freedom is effectively frozen out by the lattice potential. The sum of entropies and atom numbers of 2D gases in the vertical lattice are then fitted to give the total entropy S_0 and atom number N_0 in the dipole trap, with the chemical potential μ_0 and the temperature T as free parameters:

$$\begin{cases} S_0 = \sum_j S_j^{2D}(\mu_j, T) \\ N_0 = \sum_j N_j^{2D}(\mu_j, T), \end{cases} \quad (\text{S.3})$$

where $\mu_j = \mu_0 - \frac{1}{2}m\omega_z^2 z_j^2$ is the local chemical potential and z_j is the z -coordinate of the center of the j -th vertical lattice site. An expression for the entropy of a Fermi gas as a function of T and μ can be found for example in Ref. [S4]. The density profile in each lattice site is modeled then as a 2D finite-temperature Fermi-Dirac profile in the horizontal plane and as the Gaussian vibrational ground state in the vertical direction:

$$\begin{aligned} n_j(x, y, z) = s \frac{mk_B T}{2\pi\hbar^2} \log \left[1 + \exp\left(\frac{\mu_j}{k_B T}\right) \exp\left(-\frac{m}{2k_B T} (\omega_{x,\text{lat}}^2 x^2 + \omega_{y,\text{lat}}^2 y^2)\right) \right] \\ \times \left(\frac{m\omega_{z,\text{lat}}}{\pi\hbar}\right)^{1/2} \exp\left(-\frac{m\omega_{z,\text{lat}}}{\hbar} (z - z_j)^2\right), \end{aligned} \quad (\text{S.4})$$

where s is the number of spin components and k_B is the Boltzmann constant. Horizontal confinement frequencies in the lattice are measured to be $\omega_{x,\text{lat}} = \omega_{y,\text{lat}} = 2\pi \cdot 37.5(10)$ Hz and the vertical lattice band excitation frequency at a depth of $50 E_r$ is $\omega_{z,\text{lat}} = 2\pi \cdot 28.1(3)$ kHz, leading to a typical mean density between $4 \cdot 10^{13}$ and $8 \cdot 10^{13}$ atoms/cm³.

SPIN-EXCHANGE DYNAMICS AND TWO-BODY INELASTIC LOSSES

As briefly discussed in the main text, the difference in the symmetric and antisymmetric interaction strengths leads to an effective onsite magnetic interaction between two atoms in different electronic orbitals. For a more detailed discussion of the total Hamiltonian, see Ref. [S5]. In a single-band description, the inter-orbital onsite interaction part of the Hubbard Hamiltonian can be written as

$$H_{\text{int}} = V \sum_i n_{ie} n_{ig} + V_{\text{ex}} \sum_{imm'} c_{igm}^\dagger c_{iem'}^\dagger c_{igm'} c_{iem}, \quad (\text{S.5})$$

where the operator $c_{i\alpha m}^\dagger$ creates an atom in the state $|\alpha m\rangle$ at site i of the lattice, $\alpha = g, e$ and $m = \uparrow, \downarrow$, and $n_{i\alpha} = \sum_m c_{i\alpha m}^\dagger c_{i\alpha m}$. When the system is prepared in a superposition of the symmetric and antisymmetric states $|eg^+\rangle$ and $|eg^-\rangle$, the second term in this Hamiltonian is responsible for onsite spin-exchange oscillations. For example, the superposition state:

$$|\psi(t=0)\rangle = \frac{1}{\sqrt{2}} (|eg^+\rangle + |eg^-\rangle) = |eg\uparrow\downarrow\rangle$$

evolves as:

$$|\psi(t)\rangle = \cos\left(\frac{V_{\text{ex}} t}{\hbar}\right) |eg\uparrow\downarrow\rangle + \sin\left(\frac{V_{\text{ex}} t}{\hbar}\right) |eg\downarrow\uparrow\rangle.$$

On the other hand, the exchange is energetically inhibited when the differential Zeeman shift between $|e\rangle$ and $|g\rangle$ states produced by the external magnetic field is larger than the exchange coupling strength.

A description based on binary interactions is still suitable when atoms are loaded into a 1D optical lattice. For atoms in different electronic orbitals, two scattering channels are available, characterized by different scattering lengths a_{eg}^+

and a_{eg}^- . The interaction couples therefore the $|eg\downarrow\uparrow\rangle$ and $|eg\uparrow\downarrow\rangle$ states. This is analogous to the description given in [S6] for single-orbital non-SU(N)-symmetric spin-1 bosons. Recently, collective coherent spin dynamics was observed also in a Fermi sea under specific initial conditions [S7]. In our experiment, the gas is prepared in a $|g\uparrow\rangle$ - $|e\downarrow\rangle$ balanced mixture, and no coherence is initially present between the spin-up and spin-down Fermi seas. Strong $e - e$ pair inelastic losses are initially suppressed by Pauli blocking, but those excited state atoms which underwent the spin exchange process can collide after the spin flip, causing these atoms to rapidly leave the trap. This strong loss mechanism therefore suppresses any coherence build-up. In a single-particle density matrix representation, only diagonal elements in the $\{|g\uparrow\rangle, |g\downarrow\rangle, |e\uparrow\rangle, |e\downarrow\rangle\}$ basis are non-zero: $\rho = \text{diag}(P_{g\uparrow}, P_{g\downarrow}, P_{e\uparrow}, P_{e\downarrow})$. The evolution of the state occupations of the two electronic and spin states can therefore be approximated using a simple system of coupled rate equations (linearized in density):

$$\begin{aligned}\dot{P}_{g\uparrow}(t) &= n_0\gamma_{\text{ex}}(P_{e\uparrow}(t)P_{g\downarrow}(t) - P_{e\downarrow}(t)P_{g\uparrow}(t)) - n_0\beta_{eg}P_{g\uparrow}(t)(P_{e\uparrow}(t) + P_{e\downarrow}(t)) \\ \dot{P}_{g\downarrow}(t) &= n_0\gamma_{\text{ex}}(P_{e\downarrow}(t)P_{g\uparrow}(t) - P_{e\uparrow}(t)P_{g\downarrow}(t)) - n_0\beta_{eg}P_{g\downarrow}(t)(P_{e\uparrow}(t) + P_{e\downarrow}(t)) \\ \dot{P}_{e\uparrow}(t) &= n_0\gamma_{\text{ex}}(P_{e\downarrow}(t)P_{g\uparrow}(t) - P_{e\uparrow}(t)P_{g\downarrow}(t)) - n_0\beta_{eg}P_{e\uparrow}(t)(P_{g\uparrow}(t) + P_{g\downarrow}(t)) - n_0\beta_{ee}P_{e\uparrow}(t)P_{e\downarrow}(t) \\ \dot{P}_{e\downarrow}(t) &= n_0\gamma_{\text{ex}}(P_{e\uparrow}(t)P_{g\downarrow}(t) - P_{e\downarrow}(t)P_{g\uparrow}(t)) - n_0\beta_{eg}P_{e\downarrow}(t)(P_{g\uparrow}(t) + P_{g\downarrow}(t)) - n_0\beta_{ee}P_{e\downarrow}(t)P_{e\uparrow}(t)\end{aligned}$$

Three two-body rate coefficients are introduced: γ_{ex} is the spin-exchange rate coefficient, β_{ee} is the inelastic $e - e$ pair loss rate coefficient and β_{eg} is the inelastic $e - g$ pair loss rate coefficient. All rate coefficients are independent upon the specific spin mixture, due to the collisional SU(N) symmetry. The total initial mean density of the gas is indicated as n_0 , calculated as a weighted mean of single plane densities. Due to losses, the state populations will decrease during the evolution and need thus to be normalized to obtain relative spin populations. We fit this model to the data, with γ_{ex} , β_{eg} and $P_{g\downarrow}(0)$ as free parameters. The sum $P_{e\downarrow}(0) + P_{g\downarrow}(0)$ is fixed to the fraction of $|g\downarrow\rangle$ atoms present without applying any excitation light, which is monitored to be constant during the experimental run. $P_{g\downarrow}(0)$ accounts then for imperfection of the clock π -pulse, which leaves typically 5-10% of the $|\downarrow\rangle$ atoms in the $|g\downarrow\rangle$ state. Similarly, $P_{g\uparrow}(0)$ is fixed to the fraction $|g\uparrow\rangle$ atoms in the gas in the absence of excitation light. A 2-dimensional fitting procedure is used:

the measured relative spin state population is fitted with $P_{g\uparrow}(t)/(P_{g\uparrow}(t) + P_{g\downarrow}(t))$ and the total detected ground state atom number is fitted with $N_{0g}(P_{g\uparrow}(t) + P_{g\downarrow}(t))$, where N_{0g} is the number of ground state atoms for zero hold time.

As described in the main text, inelastic $e - e$ losses are measured separately, in order to fix the value of β_{ee} . For independent inelastic $e - g$ loss measurements, the spin-exchange was suppressed by holding the atoms at high magnetic field. A mixture of $|g\uparrow\rangle$ and $|e\downarrow\rangle$ atoms is prepared by a π -pulse in a magnetic field of 20 G and the population of the ground state was measured after a varying hold time. Loss rate coefficients are obtained by fitting data with the same rate equation model with γ_{ex} set to zero. The fit of β_{eg} yields a value in good agreement with the ones obtained by fitting this parameter together with γ_{ex} as explained above. These $e - g$ pair losses in a 2D sample involve both symmetric and antisymmetric inelastic scattering channels, and the reported β_{eg} rate is therefore an effective bulk loss rate.

* simon.foelling@lmu.de

- [S1] Mark, M. J. *et al.* Precision measurements on a tunable Mott insulator of ultracold atoms. *Phys. Rev. Lett.*, **107**, 175301 (2011).
- [S2] Mark, M. J. *et al.* Preparation and spectroscopy of a metastable Mott-insulator state with attractive interactions. *Phys. Rev. Lett.* **108**, 215302 (2012).
- [S3] Busch, T., Englert, B., Rzazewski, K., and Wilkens, M. Two cold atoms in a harmonic trap. *Found. Phys.* **28**, 549 (1998).
- [S4] Köhl, M. Thermometry of fermionic atoms in an optical lattice. *Phys. Rev. A* **73**, 031601(R) (2006).
- [S5] Gorshkov, A. V. *et al.* Two-orbital SU(N) magnetism with ultracold alkaline-earth atoms. *Nature Phys.* **6**, 289-295 (2010).
- [S6] Stamper-Kurn, D. M., and Ueda, M. Spinor Bose gases: Symmetries, magnetism, and quantum dynamics. *Rev. Mod. Phys.* **85**, 1191-1244 (2013).
- [S7] Krauser, J. S. *et al.* Giant spin oscillations in an ultracold Fermi sea. *Science* **343**, 157-160 (2014).